Journal of Physics: Condensed Matter

PAPER

Electron–electron correlations and structural, spectral and polarization properties of tetragonal $BaTiO_3$

To cite this article: Naseem Ud Din *et al* 2020 *J. Phys.: Condens. Matter* **32** 475601

IOP Publishing Journal of Physics: Condensed Matter
J. Phys.: Condens. Matter **32** (2020) 475601 (8pp) https://doi.org/10.1088/1361-648X/abaa81

Electron–electron correlations and structural, spectral and polarization properties of tetragonal $BaTiO_3$

Naseem Ud Din[1], Tao Jiang, Shima Gholam-Mirzaei, Michael Chini and Volodymyr Turkowski

Department of Physics, University of Central Florida, Orlando, FL 32816, United States of America

E-mail: naseem.din@knights.ucf.edu

Received 9 June 2020, revised 13 July 2020
Accepted for publication 29 July 2020
Published 27 August 2020

Abstract

To analyze the role of electron–electron correlation effects in structural (local-geometry), spectral and polarization properties of tetragonal $BaTiO_3$ we apply DFT + U approach. We demonstrate that the system properties drastically change when the value of the local Coulomb repulsion U crosses the critical value $U_c \approx 7$ eV. In particular, the correlation effects cause a change of the ratio of the in-plane and inter-plane Ti–O bond lengths, which results in a flip of the order of the Ti d-bands and change of the polarizability of the system. Since the consensus value of U in $BaTiO_3$ is unknown, we discuss how the obtained results may be revealed in experimental data, especially in the optical response and ultrafast charge dynamics, where effective U is dynamically tuned.

Keywords: electron–electron correlation, spectral and polarization properties, DFT + U

(Some figures may appear in colour only in the online journal)

1. Introduction

Ferroelectric perovskite $BaTiO_3$ is a non-magnetic band insulator with unfilled d-electron shells (bandgap ~3.2 eV at 300 K) that exists in five different phases—hexagonal, cubic (non-ferroelectric phase), tetragonal (under ambient conditions), orthorhombic, and rhombohedral crystal structure in decreasing-temperature order. Only the cubic phase is non-ferroelectric [1]. Barium titanate has many fascinating properties and exhibits various phenomena, such as photorefractive effects and piezoelectricity. Some perovskite oxides, including $BaTiO_3$, show spontaneous polarization at ambient temperature and pressure due to the relative displacement of the cationic and anionic sublattices inside the unit-cell [2, 3]. Conversion of strain/stress to electrical response and vice versa are very important characteristics of this and other ferroelectrics [3–8]. These and other properties are or may be used in practical applications, e.g. in capacitors, electromechanical transducers, optical devices [9], and ultraviolet sources based on high-order harmonic generation [10]. Recently, it was shown that $BaTiO_3$ can be used as a part of proposed multilevel cell memories for calculators and memory devices [11]. Lack of inversion symmetry $BaTiO_3$ is a ferroelectric with a fixed direction of polarization) helps to efficiently separate photoexcited charges (electrons and holes) in the system and makes $BaTiO_3$ a good candidate to be used in photovoltaic applications [12–14], as well as in nonlinear optics. For photovoltaic applications, though, one needs to reduce the large bandgap (the energy difference between the Ti-d and O-p levels). This can be done by doping, applying pressure or even using ultrafast laser-pulse excitations that generate a quasi-equilibrium state [15, 16] (see also reference [17] on the case of $LaTiO_3$). In general, photoexcited $BaTiO_3$ demonstrates very interesting ultrafast electronic [18] and ionic [15] dynamics. In particular, as it was shown in reference [18], there are two characteristic decay times when the system relaxes to the equilibrium. Finally, in the case of reduced geometry, $BaTiO_3$ also shows several unique and potentially useful properties, like an unconventional crystal-field splitting in thin films [19] and surface-assisted dynamical ferroelectric–paraelectric transition [20].

[1] Author to whom any correspondence should be addressed.

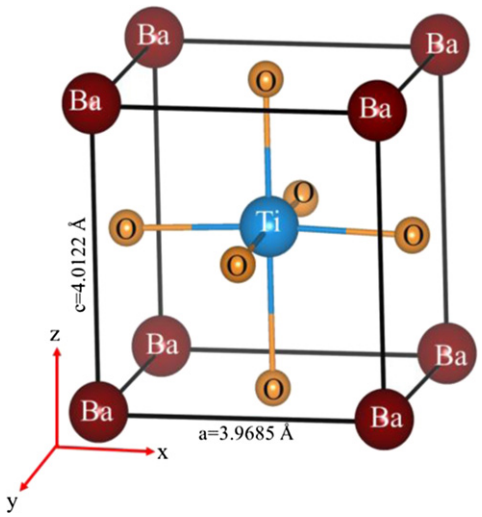

Figure 1. The unit cell of tetragonal $BaTiO_3$.

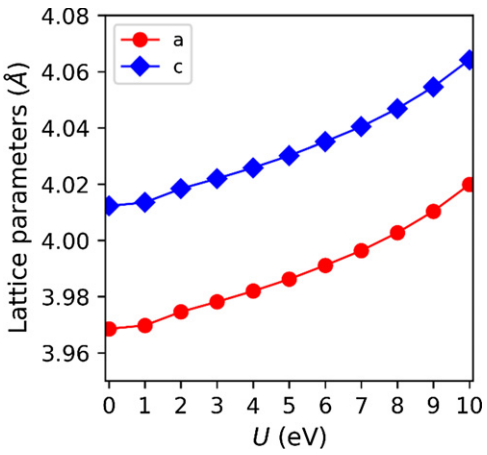

Figure 2. Optimized values of the lattice parameters of tetragonal $BaTiO_3$, as functions of the Hubbard parameter U (the experimental values for the parameters at room temperature are $a = 3.986$ A and $c = 4.026$ [40, 41]).

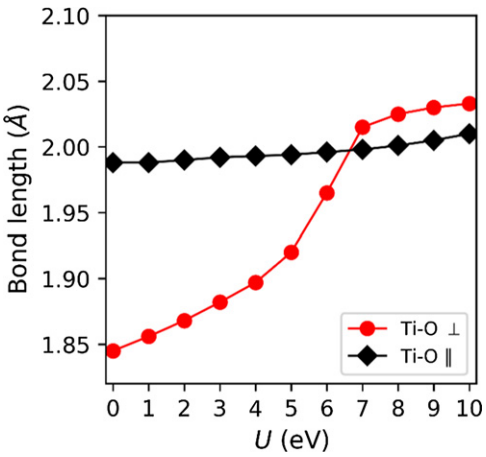

Figure 3. The Ti–O in-plane (black) and out-of-plane (red) bond lengths as functions of U (for the definitions of the in-plane and out-of-plane directions used in this paper, see figure 6).

To gain a deeper understanding of these and to predict new properties of $BaTiO_3$, it is fundamental to properly understand the spectrum and other electronic properties of the system including band ordering, density of states (DOS), electronic and optical gaps, and polarization. One of the most important steps in this tasks case is to properly take into account the effects of electron–electron correlations which are usually important in transition-metal oxides, since they have d-orbital electrons with localized charges (Ti d-orbitals in the case of $BaTiO_3$). Electron–electron interactions affect also the local geometry in the system, which define the polarization, as well as the electron dynamics and ultrafast optical response.

It is known that standard DFT approaches strongly underestimate effects of electron–electron correlations, which can result, for example, in underestimation of the electronic bandgap in $BaTiO_3$ by $\sim$1 eV with respect to the experimental value (3.2 eV). As it was shown in reference [21] one can get correct value of the gap in $BaTiO_3$ by instead using DFT + U, an approach that takes into account the local electron–electron repulsion. Here it must be noted that some alternative, advanced DFT approaches, like Heyd–Scuseria–Ernzerhof (HSE) hybrid DFT (GGA) [22], HSEsol [46], HSEint [47], and meta-GGA [48–50], can also give the correct value of the bandgap in $BaTiO_3$ [23] (see also references [24–29]). However, the physical reasoning beyond this result is not completely clear so far. Recently, several other DFT + U studies of the properties of $BaTiO_3$ were performed under different conditions and in different states, such as that of the bulk system under strain [30] and a thin film with defects [31]. Another study focusing on the properties of Mn-substituted $BaTiO_3$ was performed in reference [32] by using three different approaches—DFT, DFT + U, and its generalization DFT + DMFT that takes into account local time-resolved electron–electron interactions. It was demonstrated that such interactions lead to strong charge and valence fluctuations in the system, which are not captured by DFT and DFT + U. Otherwise, as different studies have shown, the DFT + U approach is an appropriate tool to study pure $BaTiO_3$. For example, as it was shown in another work, reference [33], this approach is a physically motivated approximation to describe free (self-trapped) O-hole polarons in $BaTiO_3$. Though, generally speaking the nature of low-energy excitations, including the mentioned polarons, and the role of local Coulomb repulsion in formation of these states in $BaTiO_3$ remain open. Several other studies of excitations in $BaTiO_3$ were performed without including these effects: within the GW approximation and solving the Bethe–Salpeter equation (that includes electron–hole coupling effects) in reference [34], and by using first-principles calculations—in reference [35].

To summarize, DFT + U studies of $BaTiO_3$ that take into account strong electron–electron correlations of $BaTiO_3$ are very limited so far, and the research has mostly focused on establishing the value of the bandgap and of the lattice parameter by using a particular value of the local Coulomb repulsion U. Moreover, besides understanding the static properties of materials there is another reason to analyze the effects of U. Namely, it is well-known that the value of the strength of the effective Coulomb interaction can dramatically change in the

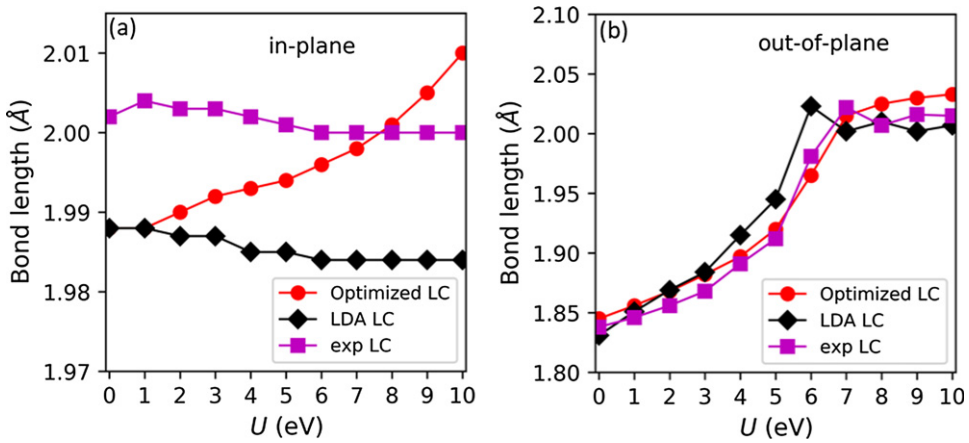

Figure 4. The Ti–O bond length in-plane (a) and out-of-plane (b) as a function of U in the case of different initial configurations: DFT (black) and experimental lattice constants [40, 41] (magenta). For comparison, the optimized-case results (red, with fixed to $U = 0$ lattice parameters) are shown in figure 3.

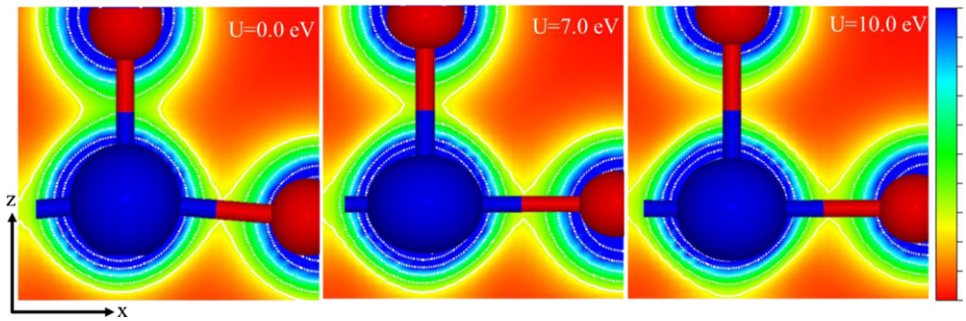

Figure 5. The xz-plane charge density in $BaTiO_3$ at different values of U. The plane crosses the in- and out-of-plane Ti and an O atom. The charge density units are arbitrary.

excited regime. As a matter of fact, the U can also strongly depend on time (see work [36] and references therein). Thus, understanding static properties of a material at different values of U, may help to understand details of the ultrafast dynamics in the system.

In this work, we perform a systematic DFT + U study of the role of U in determining the local geometry, spectral, and polarization properties of the ambient-temperature tetragonal barium titanate by tracking the evolution of these properties with increasing U. As we demonstrate, with increase of U, the system shows dramatic qualitative changes of its properties. Since the consensus value of U is unknown, we conclude with a discussion of how the obtained results can be tested experimentally in the case of ultrafast response.

2. Computational details

In this work, we have performed calculations based on DFT+U with the plane-wave and pseudo potential method as implemented in the Quantum Espresso package [37] using the LDA–PZ exchange–correlation potential [38]. The ultrasoft pseudo potentials are used to describe the core-valence interactions. The valence wave functions, and the electron density are described by a plane-wave basis set with kinetic energy cutoffs of 70 Ry and 280 Ry, respectively. In order to take into account the effects of electron–electron correlations we used the on-site Coulomb repulsion U parameter for the d-orbital electrons on the Ti atoms with values ranging from 0.0 to 10.0 eV. The Brillouin zone was sampled by using $8 \times 8 \times 8$ Monckhorst–Pack k-point grid [39] for the geometry optimization and $24 \times 24 \times 24$ grid for the band structure calculations.

We would like to note that we did not analyze the temperature effects in this work which are beyond the scope of the paper and focusing on the tetragonal phase stable at ambient conditions. Even though DFT is a zero-temperature theory, one can model different-temperature by using the corresponding experimental lattice structures as the input (and optimizing the system). Temperature effects can be also included when using, e.g., Quantum Espresso code by changing the electronic temperature (broadening) parameter that controls the occupation numbers around the Fermi energy (or in the case of semiconductors and insulators, occupation numbers at the top of valence and bottom of conduction bands), and by changing ion temperature.

3. Correlation effects and the local geometry

The unit cell of tetragonal $BaTiO_3$ is shown in figure 1, while the U-dependence of the in- and out-of-plane (in the i.e., xy-plane and perpendicular, z-direction,) lattice parameters for the relaxed structure are shown in figure 2. So far, the role of U is rather trivial: the values of the cell parameters grow

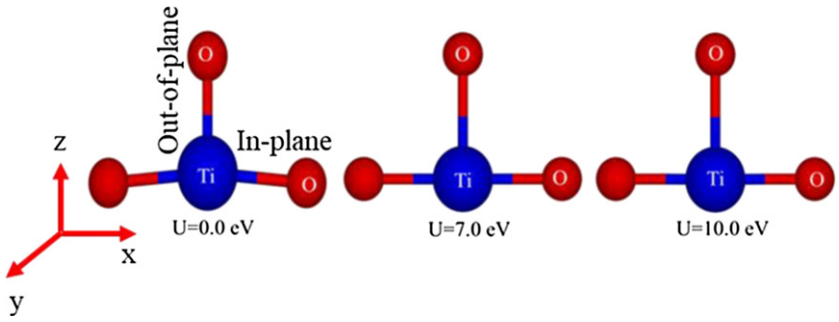

Figure 6. A qualitative representation of the U dependence of the Ti–O in- and out-of-plane plane bonds.

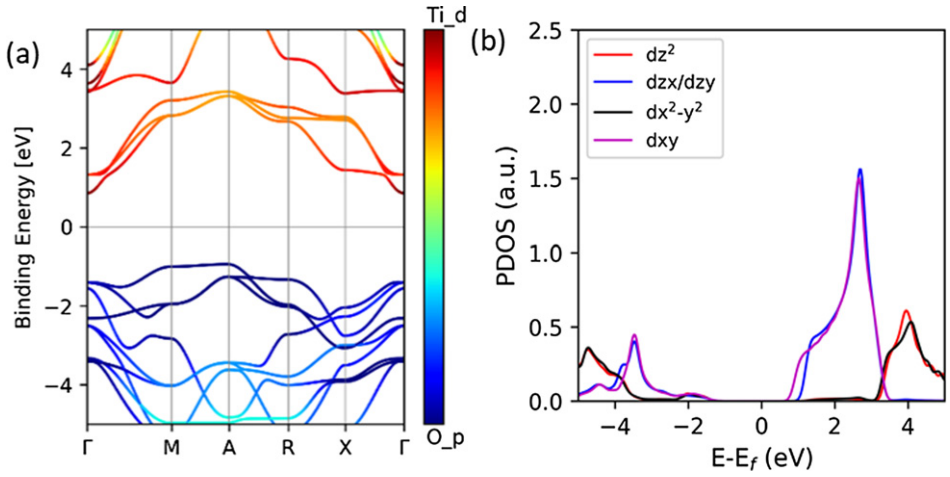

Figure 7. Orbital resolved band structure of $BaTiO_3$ (a) and projected d-orbital density of states for the Ti atoms (b) obtained by using the LDA–PZ exchange–correlation potential [38].

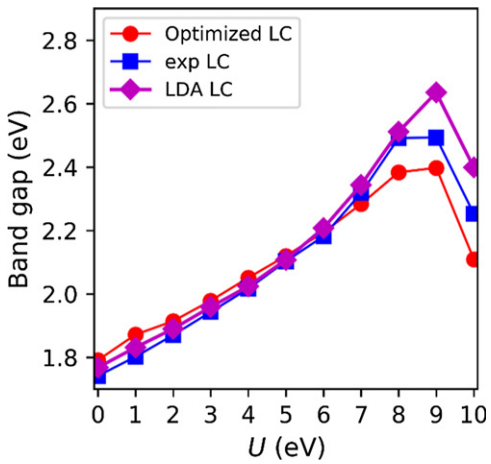

Figure 8. Calculated indirect band gap of tetragonal $BaTiO_3$ as a function of U. The results are obtained with the same computational schemes as described in caption to figure 4.

as U increases, reducing the probability of electron hopping between the correlated Ti-d orbitals, and hence reducing the energy of their on-site repulsion.

The situation is more interesting for the local geometry. In figure 3, we show dependencies of the lengths of the in-plane and out-of-plane Ti–O bonds (defined in figure 6), that play a very important role in the system polarization, as functions of U. As it follows from the figure, the out-of-plane bond length increases rapidly with increasing U, while the in-plane bond length increases much more slowly. For $U \approx 7$ eV the Ti–O in-plane and out-of-plane bond lengths become equal, and for larger values of U the out-of-plane bond length is larger than in-plane one. The significant bond length increase occurs for U values between ∼4 to 8 eV. Such a dramatic change of the out of plane bond length could significantly impact the polarization.

To test the validity of the results in figure 3, we performed the calculations using two other sets of the lattice parameters obtained from experiment (defined exp LC below) and from DFT, i.e. at $U = 0$, (LDA LC), respectively, and compared the results for the ones in figure 3 obtained with the optimized lattice parameters for each value of U (optimized LC). The U-dependence of the obtained bond lengths are shown figure 4. As it follows from this figure, the main conclusion of figure 3 holds: at $U \approx 7$ eV the out-of-plane Ti–O bond becomes larger than the in-plane one, i.e. the electron–electron correlations affect the internal geometry of $BaTiO_3$.

The charge density distributions in the O–Ti–O plane (figure 6) for three different values of U—below-critical, critical, and above-critical—are shown in figure 5. From these figures, one can clearly see the redistribution of the strength of covalent TiO bondings, from out-of-plane bond to in-plane bonds as U increases. The resulting change of the bond lengths is shown in a cartoon figure 6.

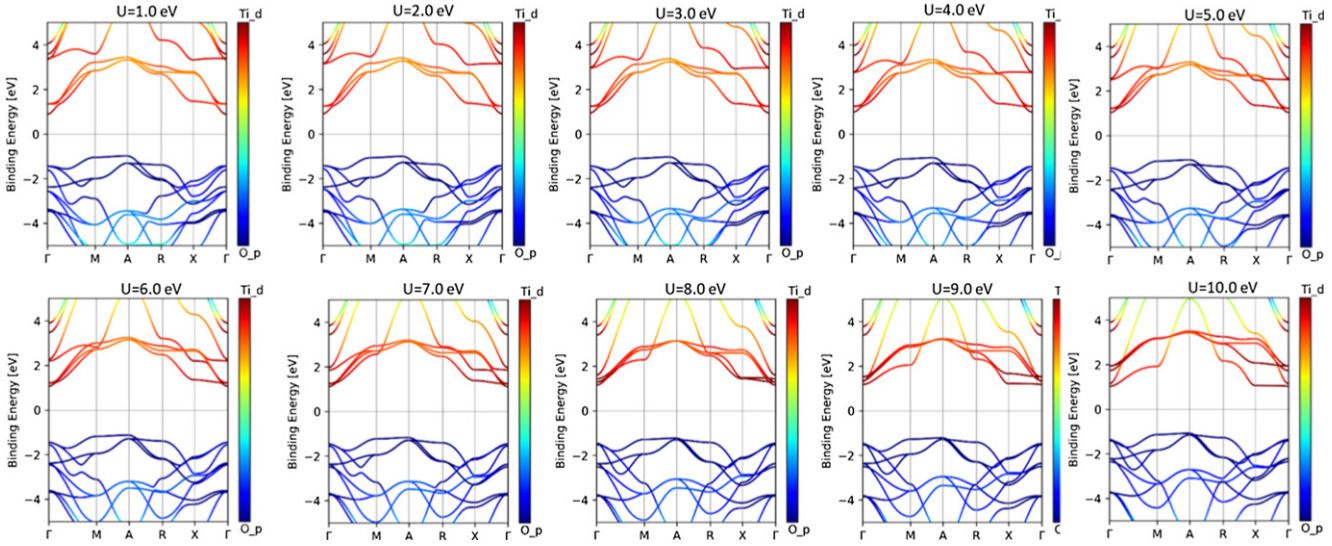

Figure 9. The dependence of the band structure of $BaTiO_3$ on U, projected into the Ti-d/O-p orbitals. In this and the next two figures, the results were obtained with the optimized lattice constants.

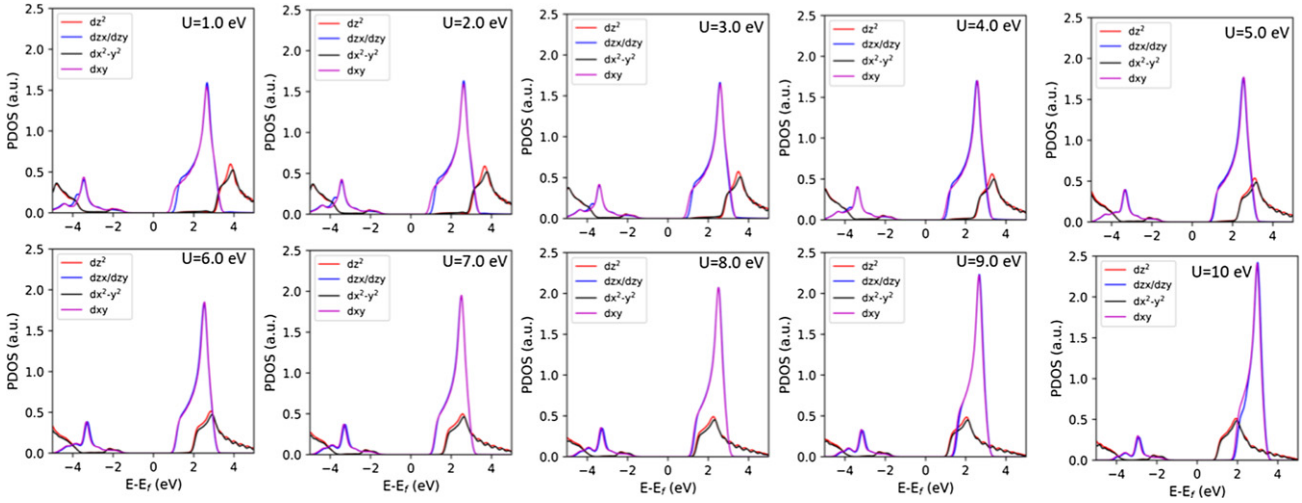

Figure 10. The projected d-orbital density of states for the Ti-d atoms at different values of U.

The reason for redistribution of the bonding strength with increasing U is connected with stronger localization of d orbitals on Ti atoms, which results in weaker hybridization between the neighboring Ti and O atom orbitals. Since the distance between the nearest Ti atoms is largest along the c axis, the hopping, and hence hybridization, gets more suppressed in this direction, and as a result the bond lengths in the c direction increase most.

4. Correlation effects and spectral properties

Results of the DFT calculations of the electronic band structure and orbital-resolved density of states show that the system is indirect-bandgap insulator with gap $\sim$1.8 eV. The valence bands are formed predominantly by hybridized oxygen p-orbital states, and the conduction bands—by titanium d-orbital states. The bottom of the conduction band consists mostly of d_{xy} electron states, indicating that low-energy excitations are xy-plane quasi-particles (i.e., excitations in the xy-plane crossing the Ti atoms, centers of the corresponding xy-plane d_{xy} orbitals, figure 6), i.e. that low-energy dynamics of the excited system occur primarily within two dimensions (figure 7).

The spectral properties of the system change dramatically as U grows from zero to 10 eV, as in the case of the bond lengths. In particular, as U becomes larger than critical value the band gap dependence on U changes from growing to decreasing (figure 8). As was the case with the bond lengths, the changes in the band gap with increasing U are stable with respect to the optimization procedure. Calculations initialized with lattice constants obtained from experiments and DFT both show similar behavior in agreement with the optimized lattice constants, though with some quantitative differences in the observed maximum band gap. Due to a rather good agreement between the results above obtained with three different sets of lattice constants, in the remaining part of the paper we present results for optimized lattice constant only.

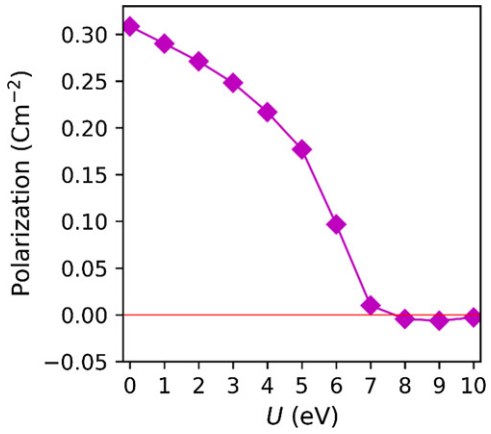

Figure 11. Out-of-plane polarization as function of U (experimental value of the room-temperature polarization directed out-of-plane is approximately 26 uC cm^{-2} [42]).

To obtain a deeper insight on the reason for such a change of the gap, we have performed calculations of the electronic band structure (figure 9) and of the projected DOS (figure 10) at different values of U. Besides decrease of the band gap, the most interesting result of figure 9 is band flattening at the X–Γ region when U becomes larger than the critical value. Much more interesting effect of U can be observed in the DOS shown in figure 9. Namely, we observe a flipping of the order of the conduction t_{2g} and e_g bands when U becomes larger than 7 eV. This is a very important result, suggesting that the in-plane ($d_{x^2-y^2}$) state will have an increased weight in the low-energy excitation spectrum, while for small U such states are predominantly of the out-of-plane (d_{zx} and d_{zy}) symmetry. Thus, the direction of the polarization and the dominant response direction of the system excited by, e.g., a laser pulse will change from the out-of-plane to in-plane as U increases.

5. Correlation effects and polarization

This result is also confirmed by calculation of polarization as function of U, as shown in figure 11. As the calculations show, the magnitude of the out-of-plane polarization dramatically decreases, and the polarization changes sign, as U becomes larger than the critical value. We find that the increase of the out-of-plane Ti–O bond length with U (figure 3) is the main reason for the accompanying decrease of polarization. Indeed, longer distance between the 'vertical' Ti–O polarization charges (i.e., their weaker coupling) favors 'leaking' of the Ti-atom charge to the left and right bonds with oxygen atoms, and hence decrease of the polarization.

6. Summary and conclusions

We have applied DFT + U approach to study the role of correlation effects in the geometric, spectral and polarization properties of tetragonal $BaTiO_3$. We have found a dramatic change in these properties as U becomes larger than a critical value of ∼7 eV. Most notably, the in-plane Ti–O bonds become shorter than the out-of-plane ones, electronic bandgap dramatically decreases, and the t_{2g} and e_g conduction bands flip order, resulting in exchange of the predominantly out-of-plane low-energy excitations to in-plane ones. The band flipping also leads to a dramatic decrease of the static polarization, originally oriented out-of-plane. All of these correlation-induced effects may play an important role in the excitation spectrum, ultrafast charge dynamics and other elements of the optical response of the system. While there is no consensus on value of the Hubbard U for $BaTiO_3$, the obtained critical value is not very far from those often used, $U = 4$–6 eV.

The main findings of the work—change of different physical quantities with U (the in-plane and out-of-plane bond lengths, band gap, band order and polarization) may be revealed in the optical spectra and ultrafast response and tested experimentally. Possible measurable effects include:

(a) Change of the transient absorption spectrum (due to change of the band gap) [43, 44].
(b) Anisotropic response, including linear and non-linear (higher-harmonic) emission, of the system to different-angle perturbations (due to different change of the in- and out-of-plane bond lengths and change of the polarization) [9].
(c) Strong dependence of the beating [45] and the oscillatory inter-orbital currents [43] on the pulse polarization (due an oscillatory time-dependence of the orbitals population [43] and the band-order flip, i.e. change of symmetry of the low-energy conduction bands).

Theoretical analysis of these and other U-dependent effects in $BaTiO_3$ is planned to be performed in near future.

Acknowledgments

We would like to thank Aiping Chen for an enlightening communication and critical comments. This work was supported by the United States National Science Foundation under Grant No. DMR-1809181.

ORCID iDs

Naseem Ud Din https://orcid.org/0000-0002-7972-4057
Tao Jiang https://orcid.org/0000-0003-0419-7288
Shima Gholam-Mirzaei https://orcid.org/0000-0002-3209-7666
Michael Chini https://orcid.org/0000-0002-9058-928X
Volodymyr Turkowski https://orcid.org/0000-0003-0762-0002

References

[1] Hayward S A and H Salje E K 2002 The pressure–temperature phase diagram of $BaTiO_3$: a macroscopic description of the low-temperature behavior *J. Phys.: Condens. Matter* **14** L599
[2] Wang J *et al* 2010 Temperature–pressure phase diagram and ferroelectric properties of $BaTiO_3$ single crystal based on a modified Landau potential *J. Appl. Phys.* **108** 114105
[3] Li Y, Cross L and Chen L 2005 A phenomenological

thermodynamic potential for $BaTiO_3$ single crystals *J. Appl. Phys.* **98** 064101
[4] Bowen C R *et al* 2014 Piezoelectric and ferroelectric materials and structures for energy harvesting applications *Energy Environ. Sci.* **7** 25
[5] Aschauer U and Spaldin N A 2014 Competition and cooperation between antiferrodistortive and ferroelectric instabilities in the model perovskite $SrTiO_3$ *J. Phys.: Condens. Matter* **26** 122203
[6] Shi J *et al* 2014 Atomic sublattice decomposition of piezoelectric response in tetragonal $PbTiO_3$, $BaTiO_3$, and $KNbO_3$ *Phys. Rev.* B **89** 094105
[7] Cross L and Newnham R 1987 History of ferroelectrics *Ceramics and Civilization* vol 3 (Westerville, OH: American Ceramic Society) p 289
[8] Vijatović M, Bobić J and Stojanović B 2008 History and challenges of barium titanate: part I *Sci. Sinter.* **40** 155
[9] Garrett M H, Chang J Y, Jenssen H P and Warde C 1992 High beam-coupling gain and deep- and shallow-trap effects in cobalt-doped barium titanate, $BaTiO_3$: Co *J. Opt. Soc. Am.* **9** 1407
[10] Gholam-Mirzaei S, Crites E, Beetar J E, Chen A and Chini M 2018 Anisotropic polarization dependent high harmonic generation in the ferroelectric crystal $BaTiO_3$ *Conference on Lasers and Electro-Optics* (San Jose)
[11] Paglan P A and Nguenang J P 2019 Modeling of multilevel cell memory with the $BaTiO_3$/Fe nanostructured multiferroic composite material *Phys. Rev.* B **100** 020404(R)
[12] Yang S Y *et al* 2010 Above-bandgap voltages from ferroelectric photovoltaic devices *Nat. Nanotechnol.* **5** 143
[13] Cao D, Wang C, Zheng F, Dong W, Fang L and Shen M 2012 High-efficiency ferroelectric-film solar cells with an *n*-type Cu_2O cathode buffer layer *Nano Lett.* **12** 2803
[14] Grinberg I *et al* 2013 Perovskite oxides for visible-light-absorbing ferroelectric and photovoltaic materials *Nature* **503** 509
[15] Chen F *et al* 2016 Ultrafast terahertz-field-driven ionic response in ferroelectric $BaTiO_3$ *Phys. Rev.* B **94** 180104
[16] Kuo Y-H, Nah S, He K, Hu T and Lindenberg A M 2017 Ultrafast light-induced symmetry changes in single $BaTiO_3$ nanowires *J. Mater. Chem.* C **5** 1522
[17] Gu M and M Rondinelli J 2016 Ultrafast band engineering and transient spin currents in antiferromagnetic oxides *Sci. Rep.* **6** 25121
[18] Acharya S, Chouthe S, Graener H, Böntgen T, Sturm C, Schmidt-Grund R, Grundmann M and Seifert G 2014 Ultrafast dynamics of the dielectric functions of ZnO and $BaTiO_3$ thin films after intense femtosecond laser excitation *J. Appl. Phys.* **115** 053508
[19] Song Y *et al* 2019 Unconventional crystal field splitting in non-centrosymmetric $BaTiO_3$ thin films (arXiv:1908.07194)
[20] Barzilay M, Elangovan H and Ivry Y 2019 Surface nucleation of the paraelectric phase in ferroelectric $BaTiO_3$: atomic scale mapping (arXiv:1908.07276)
[21] Chen H and Millis A 2017 Design of new Mott multiferroics via complete charge transfer: promising candidates for bulk photovoltaics *Sci. Rep.* **7** 6142
[22] Heyd J, Scuseria G E and Ernzerhof M 2003 Hybrid functionals based on a screened Coulomb potential *J. Chem. Phys.* **118** 8207
[23] Sun J *et al* 2016 Accurate first-principles structures and energies of diversely bonded systems from an efficient density functional *Nat. Chem.* **8** 831
[24] Bilc D I, Orlando R, Shaltaf R, Rignanese G M, Iniguez J and Ghosez P 2008 Hybrid exchange–correlation functional for accurate prediction of the electronic and structural properties of ferroelectric oxides *Phys. Rev.* B **77** 165107
[25] Wahl R, Vogtenhuber D and Kresse G 2008 $SrTiO_3$ and $BaTiO_3$ revisited using the projector augmented wave method: performance of hybrid and semilocal functionals *Phys. Rev.* B **78** 104116
[26] Liu Q-J, Zhang N-C, Liu F-S, Wang H-Y and Liu Z-T 2003 $BaTiO_3$: energy, geometrical and electronic structure, relationship between optical constant and density from first-principles calculations *Opt. Mater.* **35** 2629
[27] Goh E S, Ong L H, Yoon T L and Chew K H 2016 Structural and response properties of all $BaTiO_3$ phases from density functional theory using the projector-augmented-wave methods *Comput. Mater. Sci.* **117** 306
[28] Paul A, Sun J, Perdew J P and Waghmare U V 2017 Accuracy of first-principles interatomic interactions and predictions of ferroelectric phase transitions in perovskite oxides: energy functional and effective Hamiltonian *Phys. Rev.* B **95** 054111
[29] Lenarczyk P and Luisier M 2020 First-principles calculations for ferroelectrics at constant polarization using generalized Wannier functions (arXiv:2001.09543)
[30] Watanabe Y 2018 Calculation of strained $BaTiO_3$ with different exchange correlation functionals examined with criterion by Ginzburg–Landau theory, uncovering expressions by crystallographic parameters *J. Chem. Phys.* **148** 194702
[31] Majumder S, Basera P, Tripathi M, Choudhary R J, Bhattacharya S, Bapna K and Phase D M 2019 Elucidating the origin of magnetic ordering in ferroelectric $BaTiO_3$-delta thin film via electronic structure modification *J. Phys.: Condens. Matter* **31** 205001
[32] Mandal S, Cohen R E and Haule K 2018 Valence and spin fluctuations in the Mn-doped ferroelectric $BaTiO_3$ *Phys. Rev.* B **98** 075155
[33] Erhart P, Klein A, Aberg D and Sadigh B 2014 Efficacy of the DFT + U formalism for modeling hole polarons in perovskite oxides *Phys. Rev.* B **90** 035204
[34] Sanna S, Thierfelder C, Wippermann S, Sinha T P and Schmidt W G 2011 Barium titanate ground- and excited-state properties from first-principles calculations *Phys. Rev.* B **83** 054112
[35] Procel L M, Tipan F and Stashans A 2003 Mott–Wannier excitons in the tetragonal $BaTiO_3$ lattice *Int. J. Quantum Chem.* **91** 586
[36] Tancogne-Dejean N, Sentef M A and Rubio A 2018 Ultrafast modification of Hubbard U in a strongly correlated material: *ab initio* high-harmonic generation in NiO *Phys. Rev. Lett.* **121** 097402
[37] Giannozzi P *et al* 2009 Quantum ESPRESSO: a modular and open-source software project for quantum simulations of materials *J. Phys.: Condens. Matter* **21** 395502
[38] Perdew J P and Zunger A 1981 Self-interaction correction to density-functional approximations for many-electron systems *Phys. Rev.* B **23** 5048
[39] Monkhorst H J and Pack J D 1976 Special points for Brillouin zone integrations *Phys. Rev.* B **13** 5188
[40] Shirane G, Danner H and Pepinsky R 1957 Neutron diffraction study of orthorhombic $BaTiO_3$ *Phys. Rev.* **105** 856
[41] Bilc D I, Orlando R, Shaltaf R, Rignanese G-M, Íñiguez J and Ghosez P 2008 Hybrid exchange–correlation functional for accurate prediction of the electronic and structural properties of ferroelectric oxides *Phys. Rev.* B **77** 165107
[42] Shieh J, Yeh J H, Shu Y C and Yen J H 2009 Hysteresis behaviors of barium titanate single crystals based on the operation of multiple 90° switching systems *Mater. Sci. Eng.* B **161** 50
[43] Sandri M and Fabrizio M 2015 Nonequilibrium gap collapse near a first-order Mott transition *Phys. Rev.* B **91** 115102
[44] Jager M F, Ott C, Kraus P M, Kaplan C J, Pouse W, Marvel R E, Haglund R F, Neumark D M and Leone S R 2017 Tracking the insulator-to-metal phase transition in VO_2 with few-femtosecond extreme UV transient absorption spectroscopy *Proc. Natl Acad. Sci.* **114** 9558

[45] Turkowski V and Freericks J K 2007 Nonequilibrium perturbation theory of the spinless Falicov–Kimball model: second-order truncated expansion in *U Phys. Rev.* B **75** 125110
[46] Schimka L, Harl J and Kresse G 2011 Improved hybrid functional for solids: the HSEsol functional *J. Chem. Phys.* **134** 024116
[47] Jana S, Patra A, Constantin L A and Samal P 2020 Screened range-separated hybrid by balancing the compact and slowly varying density regimes: satisfaction of local density linear response *J. Chem. Phys.* **152** 044111
[48] Tran F and Blaha P 2009 Accurate band gaps of semiconductors and insulators with a semilocal exchange–correlation potential *Rev. Lett.* **102** 226401
[49] Patra B, Jana S, Constantin L A and Samal P 2019 Efficient band gap prediction of semiconductors and insulators from a semilocal exchange–correlation functional *Phys. Rev.* B **100** 045147
[50] Aschebrock T and Kümmel S 2019 Ultranonlocality and accurate band gaps from a meta-generalized gradient approximation *Phys. Rev. Res.* **1** 033082